Phonon-Activated Collective Hopping in a Superionic Phase

Hung-Min Lin,[1] Mayanak K. Gupta,[2,3] Niuchang Ouyang,[4] Tyler Wilson,[5] Artem Pogodin,[6] Md Towhidur Rahman,[7] Alexandra Zevalkink,[8] J. Ross Stewart,[9] Fanni Juranyi,[10] Tao Hong,[11] Yan Wu,[11] Songxue Chi,[11] Douglas L. Abernathy,[11] and Olivier Delaire[1,4,5]

[1]*Department of Chemistry, Duke University, Durham, North Carolina 27708, USA*
[2]*Solid State Physics Division, Bhabha Atomic Research Centre, Mumbai 400085, India*
[3]*Homi Bhabha National Institute, Anushaktinagar, Mumbai 400094, India*
[4]*Department of Mechanical Engineering and Materials Science, Duke University, Durham, North Carolina 27708, USA*
[5]*Department of Physics, Duke University, Durham, North Carolina 27708, USA*
[6]*Inorganic Chemistry Department, Uzhhorod National University, Uzhhorod, 88000, Ukraine*
[7]*Department of Mechanical Engineering, Michigan State University, East Lansing, Michigan 48824, USA*
[8]*Department of Chemical Engineering and Materials Science, Michigan State University, East Lansing, Michigan 48824, USA*
[9]*ISIS Neutron and Muon Source, STFC Rutherford Appleton Laboratory, Didcot, OX11 0QX, United Kingdom*
[10]*PSI Center for Neutron and Muon Sciences, 5232 Villigen PSI, Switzerland*
[11]*Neutron Scattering Division, Oak Ridge National Laboratory, Oak Ridge, Tennessee 37831, USA*

(Received 16 December 2025; accepted 29 June 2026; published 21 August 2026)

Superionic conductors are fascinating systems representing a state of matter intermediate between solids and liquids, yet their underlying physics remain poorly understood. Correlations in jump dynamics have been theoretically proposed as a key mechanism underlying superionic diffusion, but a direct experimental demonstration remains elusive. Here, we report the direct observation of collective cation hopping in the argyrodite compound Cu_7PS_6, using single-crystal neutron scattering to access the full four-dimensional space-time correlations of ionic motion. By leveraging the rarely used coherent scattering channel in quasielastic neutron scattering, together with diffuse scattering, we reveal pronounced short-range dynamical correlations between diffusing Cu ions, providing direct experimental evidence of collective hopping in a superionic phase. Machine-learned molecular dynamics simulations quantitatively reproduce all our measurements and pinpoint the dominant collective hopping mechanism. Furthermore, we establish through both experiments and simulations that the collective diffusive hops originate from the breakdown of low-energy phonons dominated by the Cu motions in the parent ordered phase, demonstrating a key link between phonon precursors and the activation of facile collective hops. This work presents the first direct experimental evidence of collective hopping in superionic argyrodites and identifies wave-vector-resolved soft phonons as its physical origin, advancing the microscopic understanding of ionic transport in superionic solids.

DOI: 10.1103/lx5w-x6wl

Subject Areas: Condensed Matter Physics, Energy Research, Statistical Physics

I. INTRODUCTION

Superionic conductors (SICs) constitute a unique class of condensed matter systems in between liquids and solids, featuring highly mobile ions with liquidlike diffusivity within a rigid framework [1,2]. SICs could enable a wide range of important technologies, from all-solid-state batteries to fuel cells and ionotronic devices [3–5]. Yet, a deeper understanding of the microscopic mechanisms underlying the emergence of the superionic regime is needed for the rational design of next-generation SICs [6–8]. Among many proposed mechanisms, collective diffusion has emerged as a core paradigm enabling superionic conductivities [9–14]. Concerted ionic hopping could help lower migration barriers, thereby facilitating diffusion [10–12], and could also increase charge diffusivity compared to tracer diffusivity, directly improving the conductivity [13]. Collective ionic diffusion could be a

widespread phenomenon, as suggested by recent systematic machine-learning analyses of a variety of fast ion conductors [14]. However, the direct experimental probing and assessment of these theoretical predictions has remained a formidable challenge, requiring the selective measurement of four-dimensional (4D) space-time correlations in the motions of mobile ions.

Commonly used experimental techniques, such as nuclear magnetic resonance and electrochemical impedance spectroscopy, typically probe only single-particle dynamics or macroscopic transport properties and lack the spatial (or wave-vector) resolution to resolve spatially correlated ionic diffusion [15]. While dielectric and optical experiments have been used to suggest temporally correlated hops in ionic conductors, these methods rely on indirect signatures and provide limited information about ion-ion correlations [16,17]. In contrast, neutron scattering offers a powerful approach to probe ionic diffusion, as well as crystal structure and lattice dynamics, by directly accessing 4D spatiotemporal correlations of atomic motions. These correlations are encoded in the Van Hove correlation function [18], defined as

$$G(\mathbf{r},t)=\frac{1}{N}\left\langle\sum_{i,j}\delta(\mathbf{r}-\mathbf{R}_j(t)+\mathbf{R}_i(0))\right\rangle, \qquad (1)$$

which gives the probability of finding a particle at position $\mathbf{r}$ at time t, given that a reference particle was located at the origin at $t=0$. The Van Hove correlation can be decomposed into self and distinct contributions:

$$G(\mathbf{r},t)=G_s(\mathbf{r},t)+G_d(\mathbf{r},t), \qquad (2)$$

where the self ($i=j$) and distinct ($i\neq j$) contributions describe individual atomic motion and correlations between different atoms, respectively, and are selectively accessed via incoherent and coherent neutron scattering channels [19,20]. Revealing the full details of collective ionic diffusion, however, requires measuring coherent scattering channels on single crystals with wave-vector ($\mathbf{Q}$)-resolved information, which is orientationally scrambled in more common measurements on powders [21,22]. Even in rare single-crystal quasielastic neutron scattering (QENS) studies, the focus has predominantly been on self-diffusion through incoherent scattering [23,24]. Comprehensive coherent QENS (c-QENS) studies on superionic crystals are thus highly desirable to resolve the microscopic physics underpinning the collective diffusion mechanism. This demands state-of-the-art neutron spectroscopy measurements on large, high-quality single crystals, complemented with thorough analysis of the complex 4D $S(\mathbf{Q},E)$, to probe and rationalize the key dynamical timescales and spatial correlations.

Argyrodites with the general composition A_7PCh_6 (A = Li, Cu, Ag; Ch = S, Se) have emerged as a widely studied class of superionic compounds, owing to their remarkable ionic diffusivity, but their structural complexity and multiple diffusion pathways have challenged both experiments and simulations [25–29]. Computational studies have predicted that ion diffusion in argyrodites is highly correlated, yet direct experimental evidence remains lacking [28,30–32]. Beyond collective ion hops, further dynamical correlations between the hops of mobile ions and phonon modes of the framework lattice could also enable fast ion transport [33,34]. These included considerations of soft lattice [35,36], phonon anharmonicity [37–39], and a so-called paddle-wheel scenario [40]. However, it remains highly debated which dynamical correlations are key for ionic transport, with controversy surrounding the paddle-wheel effect [33,41,42]. Indeed, atomistic simulations point to the absence of a paddle-wheel mechanism in argyrodites, suggesting that other dynamical correlations are at play [26,27]. Inelastic neutron scattering (INS) measurements on powder samples of several argyrodites found softening and broadening of low-energy phonons across the superionic transition, suggesting that some particularly soft and anharmonic phonon modes may act as precursors to ionic hopping [26–29]. Recent work on Li_6PS_5Cl [27] further showed that overdamped low-energy phonons lead to a linear DOS, the characteristic signature of liquid diffusion described by the instantaneous normal mode framework [43–45]. These findings reveal the presence of liquidlike dynamics in superionic argyrodites and point to their intrinsic origin in strongly anharmonic phonons. However, powder-based measurements inherently obscure mode-resolved information, leaving open the central question of which specific phonon modes are most strongly involved in the emergence of a superionic phase. Moreover, although low-energy phonons have been proposed to encode minimum energy pathways for ion migration, whether collective vibrational modes are the origin of correlated ion hopping has remained unclear [46–48].

To directly assess the extent of cooperativity of ionic hops and identify the key dynamical correlations underlying facile ionic transport, we performed extensive neutron scattering measurements and large-scale machine-learned molecular dynamics (MLMD) simulations on the argyrodite Cu_7PS_6, which becomes superionic above an order-disorder transition at 510 K [49,50]. Copper ions present a unique advantage for neutron scattering investigations, possessing both incoherent ($\sigma_{inc}=0.55$ b) and coherent ($\sigma_{coh}=7.485$ b) scattering cross sections, which provides access to both single-particle and collective ionic dynamics [51]. By leveraging the full capability of neutron scattering, here we report the first direct observation of collective hopping in superionic argyrodites and trace its origin to strongly anharmonic phonons. Our measurements on high-quality single crystals reveal prominent $\mathbf{Q}$-dependent

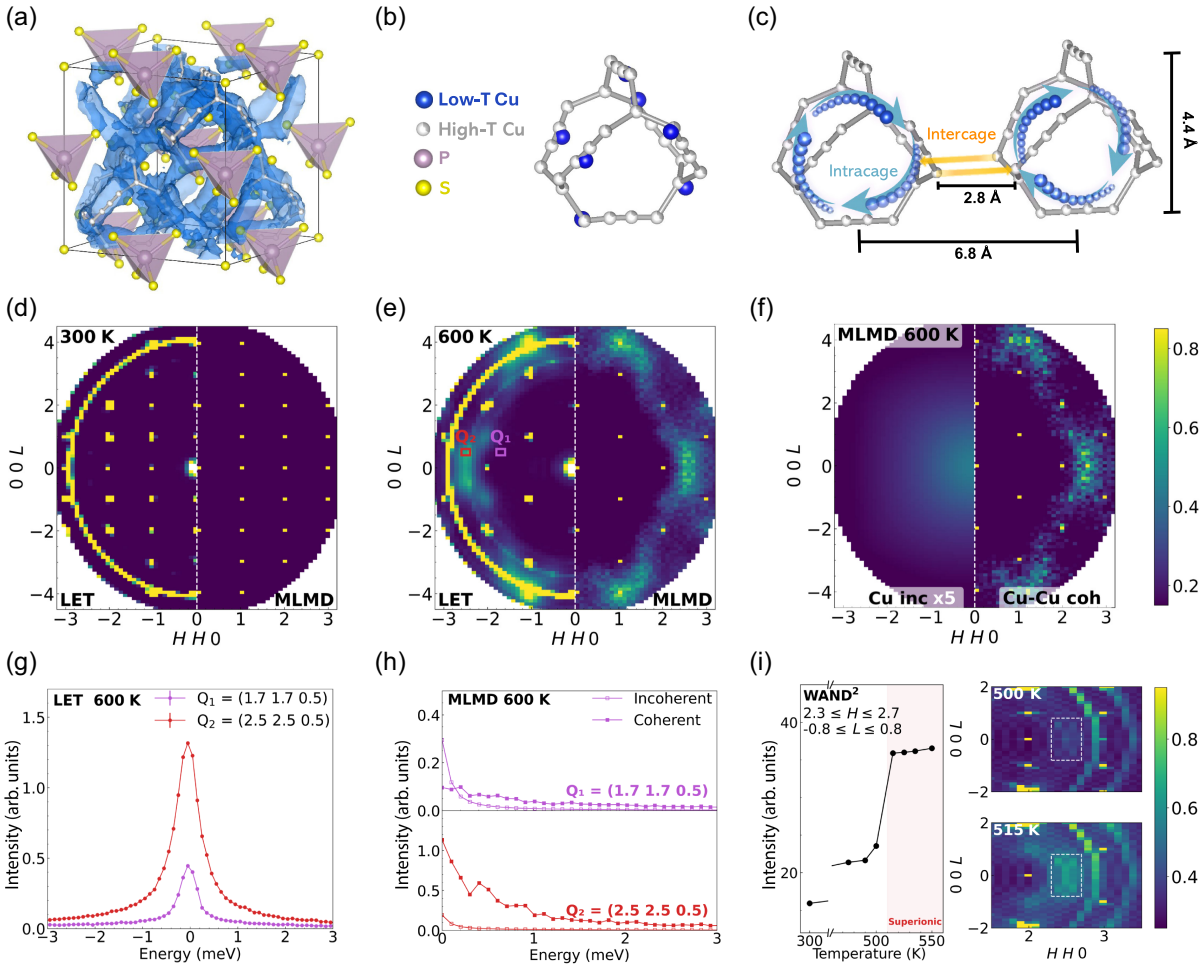

FIG. 1. Coherent QENS revealing collective hopping in the superionic Cu_7PS_6. (a) Crystal structure of Cu_7PS_6 in the superionic phase, with Cu probability density (blue clouds) visualized from 600 K MLMD trajectories. (b) Overlay of Cu sites in the normal phase and partially occupied Cu sites in the superionic phase for a representative cage. (c) Schematic illustration of intracage and intercage pathways in Cu_7PS_6. Intracage jump in argyrodites is predicted to be highly correlated. (d),(e) Elastic intensity maps in the $(H\,H\,L)$ plane ($|E| \leq 1$ meV) from LET measurements (left) and MLMD simulations (right) at (d) 300 and (e) 600 K, showing the emergence of diffuse scattering lobes in the superionic phase, particularly around $\mathbf{Q} = (2.5\,2.5\,0)$ and (1 1 4). The ring in LET data is from diffraction by the aluminum sample holder. (f) $S(\mathbf{Q})$ maps in the $(H\,H\,L)$ plane for $|E| \leq 1$ meV from the Cu incoherent contribution (left) and the Cu-Cu coherent contribution (right), calculated from 600 K MLMD trajectories. The intensity of the Cu incoherent contribution is multiplied by 5 to highlight the feature. (g) Representative $S(E)$ spectra at 600 K from LET at $\mathbf{Q}_1 = (1.7\,1.7\,0.5)$, off the diffuse lobes, and $\mathbf{Q}_2 = (2.5\,2.5\,0.5)$, on the diffuse lobes, revealing a stronger QENS response at $\mathbf{Q}_2$. (h) Corresponding MLMD-simulated $S(E)$ spectra at the same $\mathbf{Q}$ points, separated into coherent and incoherent components, showing the strong coherent QENS contribution at $\mathbf{Q}_2 = (2.5\,2.5\,0.5)$. (i) Temperature-dependent intensity of diffuse lobes around (2.5 2.5 0) from WAND^2 measurements, with maps at selected temperatures just below and above the T_c, highlighting the sharp emergence of diffuse scattering upon entering the superionic phase.

dynamic diffuse scattering intensity between Bragg peaks, emerging in the superionic phase, from which we are able to directly resolve the nature of spatial correlations between diffusive Cu ions. Furthermore, our QENS measurements resolve the single-ion dynamics via incoherent QENS (dominant at low $|\mathrm{Q}|$) probing the self Van Hove function, $G_s(\mathbf{r}, t)$, and the pairwise cooperative diffusive dynamics for larger $\mathbf{Q}$ associated with local processes [coherent QENS probing the distinct Van Hove function, $G_d(\mathbf{r}, t)$]. Our extensive atomistic simulations reproduce the experimental observations of all QENS components and further provide real-space insights into the collective hopping mechanism, showing that cations hop in concert while maintaining a short-ranged Cu-Cu ordering pattern. Finally, we reveal that this behavior originates from the breakdown of phonon quasiparticles, establishing a direct connection between soft anharmonic collective vibrations of the parent phase and concerted ionic hopping in the superionic regime. Together, these results establish the crucial dynamical correlations underpinning superionic transport in crystals, offering a fundamental framework for understanding and designing novel SICs.

II. COLLECTIVE HOPPING PROBED BY COHERENT QENS

The crystal structure of Cu_7PS_6 has been investigated by x-ray diffraction [49,50]. At room temperature, Cu_7PS_6 crystallizes in the normal cubic $P2_13$ phase, comprising a framework of PS_4^{3-} tetrahedra and free S^{2-} ions, with Cu ions fully occupying the Wyckoff 4a and 12b sites. Above the phase transition at $T_c = 510$ K into the superionic $F\bar{4}3m$ phase, the Cu ions become disordered and hop through three partially occupied sites (48h, 48h, and 16e) [50]. Importantly, the spatial probability density of Cu ions is very broad, forming an extended continuum as illustrated in Fig. 1(a), evidence of a shallow underlying potential energy surface. The partially occupied Cu sites in the superionic phase form cagelike clusters, with each unit cell of Cu_7PS_6 containing four such cages. Additional structural renderings are provided in Figs. S3 and S4 [52]. Figure 1(b) compares the ordered Cu sites in the normal phase with the partially occupied sites in the superionic phase for a representative cage. Each cage has a truncated tetrahedral geometry with six edges yet accommodates seven Cu ions. This arrangement prevents all Cu ions from occupying equivalent or equidistant sites, resulting in a geometrically frustrated configuration, with the shortest Cu-Cu distance being around 2.9 Å [Figs. S3(b) and S5 [52]]. As shown schematically in Fig. 1(c), two main pathways are combined to achieve long-range facile diffusion in argyrodites, with intracage process referring to mobile ions exploring multiple sites within a single cage and intercage process describing hops between cages. Previous computational studies of argyrodites suggested that intracage hops are highly correlated [30,31].

A. Emergence of diffuse scattering and coherent QENS in superionic phase

We first report the experimental signature of collective hopping in superionic Cu_7PS_6 from single-crystal neutron scattering. Figures 1(d) and 1(e) show elastic maps measured on the LET spectrometer at the ISIS Neutron and Muon Source at 300 K in the normal phase and at 600 K in the superionic phase. The data confirm the high quality of our crystal and clearly capture the structural transition from simple cubic to face-centered cubic (only all-even or all-odd Miller indices allowed above T_c). Importantly, a clear **Q**-dependent diffuse scattering signal emerges in-between Bragg peaks in the superionic phase, forming several lobes including local intensity maxima around (1 1 4) and (2.5 2.5 0) in the horizontal scattering plane, as well as in vertical planes (Fig. S7 [52]). To rationalize these observations, we performed large-scale MLMD simulations with machine-learned potentials trained on *ab initio* data. This approach enables larger and longer simulations while maintaining near density-functional-theory-level accuracy. The simulations were run on a $10 \times 10 \times 10$ supercell (56 000 atoms) to achieve the momentum resolution of 0.1 in reciprocal lattice units (r.l.u.), allowing direct comparison with the neutron measurements. Our MLMD simulations successfully reproduce the diffuse scattering lobes [see Figs. 1(d), 1(e), S6(a), and S7 [52]] and further reveal that this signal originates exclusively from Cu-Cu pair correlations (Fig. S8 [52]). Consistent diffuse signals are seen in energy-integrated neutron diffraction measurements performed over an extended **Q** range and for additional temperatures with $WAND^2$ at the high flux isotope reactor (HFIR), which show the same diffuse lobes as LET in the horizontal plane [Figs. 1(i) and S9 [52]]. Furthermore, the $WAND^2$ data show a decay of diffuse intensity at higher $|Q|$, consistent with angstrom-scale correlations, and reveal an abrupt temperature dependence, with diffuse lobes suddenly appearing in the superionic phase.

The diffuse lobes in the superionic phase reflect the existence of prominent short-range Cu-Cu correlations, despite Cu ions hopping dynamically across many sites. Indeed, these correlations are dynamic in nature, unlike the static short-range disorder often discussed in diffraction measurements. Figure S10 [52] shows the $S(\mathbf{Q})$ maps with different E-integration ranges from LET data, demonstrating the dynamic nature of the diffuse signal, which exhibit a finite energy component extending beyond the elastic channel. These results indicate dynamically correlated disorder and suggest that Cu-Cu pairs tend to hop collectively while preserving short-range spatial correlations. Since coherent scattering arises from interference between neutron wavelets scattered by different atoms, it is sensitive to relative atomic positions and produces structured **Q**-dependent intensity in reciprocal space. In contrast, incoherent scattering probes only the self-correlation of individual atoms and therefore produces smoothly varying intensity distribution. Therefore, the intensity maxima observed for **Q** vectors on diffuse lobes, with their associated quasielastic response, demonstrate the presence of coherent QENS, as expected from the dominantly coherent scattering length of Cu [19,63]. This interpretation is supported by the MLMD calculations shown in Fig. 1(f), where the Cu incoherent and Cu-Cu coherent contributions to the $S(\mathbf{Q})$ maps are presented separately (the intensity of the Cu incoherent contribution is multiplied by 5 to make the feature more visible; for the same intensity scale, see Fig. S11 [52]). These demonstrate that the observed **Q**-dependent diffuse intensity originates predominantly from the Cu-Cu coherent contribution. To further illustrate this, we compare the spectra at two representative **Q** points $\mathbf{Q}_1 = (1.7\,1.7\,0.5)$, away from the diffuse lobes, and at $\mathbf{Q}_2 = (2.5\,2.5\,0.5)$, on a diffuse lobe, respectively. As shown in Fig. 1(g), the QENS signal extends up to a few meV at both **Q** at 600 K. This broadening, which significantly exceeds the instrumental resolution of 0.28 meV [Figs. 2(c) and 2(d)], reflects rapid relaxational dynamics of Cu ions from stochastic hopping in the

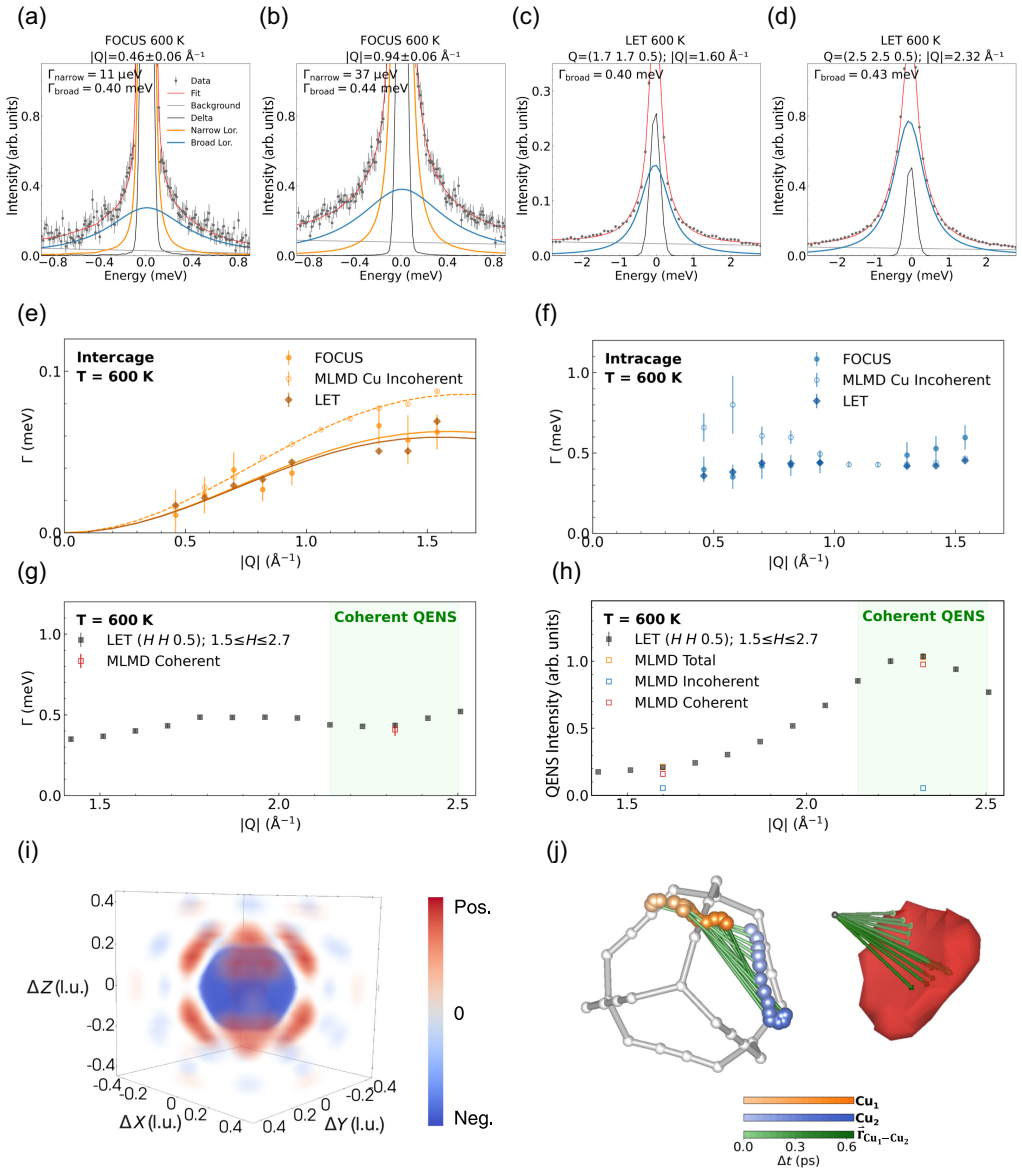

FIG. 2. Resolving the diffusion processes in Cu_7PS_6 including long-range intercage jump, restricted intracage jump, and collective behavior emerging during intracage jump. (a)–(d) Representative QENS spectral fits at 600 K. QENS widths are reported as half width at half maximum (HWHM). (a),(b) High-resolution powder QENS measurements at low-|Q| region with FOCUS resolve two QENS components with distinct timescales, corresponding to slow and fast hopping processes. (c),(d) LET single-crystal measurements at higher **Q** around the diffuse scattering capture the broader component. (e),(f) The slow and fast components extracted from FOCUS exhibit (e) |Q|-dependent broadening following the Chudley-Elliott model (curves), consistent with long-range intercage diffusion, and (f) |Q|-independent broadening, indicative of localized intracage motion. MLMD simulations reproduce these features and confirm that the QENS broadening in the low-|Q| region arises primarily from incoherent scattering due to Cu self-diffusion. The two distinct QENS components are likewise observed in the LET single-crystal measurements with $E_i = 1.91$ meV. (g) QENS widths extracted from LET measurements along the $[H\,H\,0.5]$ direction, with the green shading indicating the region where diffuse scattering and coherent QENS are observed. LET measurements yield the same |Q|-independent width as in (f), confirming that the observed dynamics are associated with intracage process, but further reveal coherent QENS features at specific **Q** points, highlighting the presence of collective hopping. (h) QENS intensity along the $[H\,H\,0.5]$ direction at 600 K from LET measurements and MLMD simulations, showing a clear **Q** dependence with stronger intensity at specific **Q** regions arising from coherent QENS. The QENS intensity from LET is obtained from the integrated area of the fitted Lorentzian components shown in Fig. S35 [52]. The intensity from MLMD is obtained from the integrated area of $S(E)$ in the quasielastic region shown in Fig. 1(h), excluding the elastic line. (i) Calculated 3D Δ-PDF from 600 K MLMD reveals strong positive Cu-Cu correlations along specific bond vectors near [0.15 0.15 0.25], indicating spatially correlated hopping. (j) MLMD trajectories confirm that Cu ions undergo collective intracage jump while preserving a specific set of Cu-Cu bond vectors. Left: a representative two-ion collective hop from 600 K MLMD. Only frames corresponding to a correlated hop are shown for clarity (time step between frames shown is 0.04 ps). Right: temporal evolution of the Cu-Cu bond vector during this event, overlaid on the strong correlation feature in the 3D Δ-PDF.

superionic phase. Importantly, the QENS intensity at (2.5 2.5 0.5), where diffuse scattering is observed, is much stronger. MLMD simulations reproduce the observed phenomenon and allow us to separate the incoherent and coherent contributions [Figs. S6(b) [52] and 1(h)]. Pronounced coherent QENS is observed at (2.5 2.5 0.5), in contrast to (1.7 1.7 0.5). This confirms that the stronger QENS intensity at (2.5 2.5 0.5), which is the dynamic component of the diffuse signal, originates from c-QENS.

Generally, ion diffusion is studied by incoherent QENS, which provides microscopic information about self-diffusion alone. The observation of coherent QENS in ionic hopping systems reflects spatially correlated ionic jumps, indicative of a collective hopping mechanism [19,22,64–68]. It should be noted, however, that coherent QENS reflects overdamped correlated dynamics and is not *a priori* associated with collective hopping (see discussion in Appendix B). Yet, in the present case of Cu_7PS_6, the coherent QENS signal emerges specifically in the superionic phase, concomitant with the onset of rapid Cu-ion hopping. We further show that the coherent QENS observed with INS matches, in both $\mathbf{Q}$ and E, the MLMD simulations. The signal arises from spatial correlations associated with the cooperative Cu hopping process. Additional discussion of the interpretation of coherent QENS as a signature of collective hopping behavior is provided in Appendix B. Together, our neutron scattering measurements and MLMD simulations reveal $\mathbf{Q}$-dependent diffuse scattering with coherent QENS in superionic Cu_7PS_6, providing experimental evidence of its collective hopping behavior. We note that polarized neutron measurements can, in principle, provide a separation of coherent and incoherent scattering contributions [64,69]. However, such measurements remain extremely slow and therefore impractical to map $S(\mathbf{Q}, E)$ on single crystals while maintaining the resolution needed for QENS. Here, by leveraging a single crystal with Cu as a strong coherent neutron scatterer, we identify c-QENS through its pronounced $\mathbf{Q}$ dependence without requiring polarization analysis [see intensity difference in calculated $S(\mathbf{Q})$ from Cu incoherent and Cu-Cu coherent contributions in Fig. 1(f)]. Our measurements represent the first comprehensive mapping of $S(\mathbf{Q}, E)$ in a high-quality superionic argyrodite crystal, unambiguously revealing diffuse scattering features associated with correlated dynamic disorder in the superionic phase.

III. REAL-SPACE INSIGHTS INTO COLLECTIVE HOPPING

A. Resolving the diffusion processes from incoherent and coherent QENS

We next demonstrate that the observed fast coherent QENS arises from collective behavior during intracage process, while a slower incoherent QENS at low |Q| captures the long-range self-diffusion. To resolve slower diffusion processes in Cu_7PS_6, we performed QENS measurements on a powder sample using FOCUS at Swiss Spallation Neutron Source, with an instrumental energy resolution of 80 μeV at a series of temperatures. The T-dependent spectra from FOCUS (Fig. S12 [52]) show a clear QENS broadening upon warming above T_c. Figures 2(a) and 2(b) show representative fits of FOCUS spectra measured at 600 K. A delta function represents elastic scattering, and two Lorentzian components are used to capture QENS contributions, with all fit components convolved with the instrument resolution. Notably, the spectra are well described by two Lorentzian components with distinctly different widths, indicating the presence of two separate diffusion processes. The width of the broad component does not vary substantially with increasing |Q|, while the narrow one broadens, consistent with localized vs long-range diffusion [19,20]. Our MLMD simulations reproduce these observations and further establish that the FOCUS data primarily reflect the self-diffusion of Cu ions (Supplemental Material [52] Sec. IV). Figures 2(e) and 2(f) summarize the |Q|-dependent QENS widths of the two processes identified in the FOCUS measurements and simulations. The narrower component follows a Chudley-Elliott jump diffusion model, consistent with long-range diffusion on a periodic lattice [70]. The corresponding jump distance, residence time, and diffusivity are summarized in Table I. The extracted jump length of approximately 2.8 Å matches the shortest intercage Cu-Cu distance (Fig. S5 [52]), and the diffusivity, on the order of 10^{-5} cm^2/s, is consistent with previous reports in argyrodites [26–29]. We therefore infer that this slower process is being limited by intercage process. In contrast, the width of the broader component is approximately 0.4 meV, corresponding to a timescale of about 1.6 ps, which is about 10 times faster than the slower process, and exhibits no |Q| dependence, a characteristic of localized motions within a confined volume [19,20,71]. This broader component is therefore assigned to fast intracage jump, where Cu ions rapidly explore multiple sites within a single cage, but sensed through the incoherent scattering process from individual ions. The two distinct diffusion processes can be clearly illustrated by the calculated $G_s(r, t)$ for Cu ions from 600 K MLMD trajectories

TABLE I. Hopping distances, residence time, and diffusion coefficients of the intercage process at 600 K. These values are extracted based on the Chudley-Elliott fit of QENS spectra.

	FOCUS	MLMD
d_{jump} (Å)	2.8 ± 0.3	2.7 ± 0.1
τ (ps)	12.8 ± 1.2	9.3 ± 0.2
D ($\times 10^{-5}$ cm^2/s)	1.04 ± 0.32	1.31 ± 0.14

(Fig. S14 [52]). At short timescales (within 2 ps), Cu ions hop by around 3 Å, the characteristic jump length of the intracage hopping process. The correlation remains at 3–4 Å over longer times, meaning that the ion remains confined within the same cage. After about 20 ps, a new component appears around 6 Å, separated by a gap from the intracage regime, indicating the onset of intercage hopping onward to long-range transport. We note that the QENS signal from FOCUS is in quantitative agreement with our LET single-crystal measurements ($E_i = 1.91$ meV, resolution = 60 μeV) after powder averaging, further strengthening our analysis. Additional details regarding QENS analysis and diffusive characteristics are provided in Supplemental Material [52] Sec. V.

After establishing the diffusive characteristics of intercage and intracage processes from FOCUS data and MLMD, we now analyze the QENS widths from LET measurements to determine which process gives rise to the coherent signal. Figure 2(g) shows the |Q| dependence of the QENS width from LET data along the $[H\,H\,0.5]$ direction across the diffuse lobes. The QENS width shows little |Q| dependence (constant ∼0.4 meV), matching the broad component associated with intracage jump observed with FOCUS. Notably, the QENS intensity exhibits a clear **Q** dependence, with stronger response at specific **Q**, a signature of coherent QENS [Fig. 2(h)]. This is further supported by our MLMD simulations, which clearly show that the coherent QENS intensity peaks at the locations of the diffuse lobes, leading to the observed **Q**-dependent QENS intensity, whereas the incoherent QENS exhibits only weak **Q** dependence, with little intensity in the high-**Q** region where the diffuse lobes are observed [see Fig. 1(f), which shows that the incoherent QENS intensity is much stronger at low **Q**]. The same QENS width is observed in **Q** regions where coherent QENS emerges, indicating that the coherent QENS originates from the intracage process. This is further supported by the calculated distinct Van Hove correlation function $G_d(\mathbf{r}, t)$, which captures the rapid decay of Cu-Cu pair correlations consistent with collective intracage jump (see Supplemental Material [52] Sec. VI). We further characterized the temperature dependence of the coherent QENS at (2.5 2.5 0.5) from CTAX measurements at HFIR, yielding an activation energy of around 90 meV for the collective hopping process (Supplemental Material [52] Sec. VII). We note that the intracage process is reflected in both incoherent and coherent QENS channels. The incoherent signal provides the observation of single-particle dynamics of Cu ions, while the coherent part captures correlations in Cu hops within cages. Our single-crystal QENS measurements thus directly reveal the collective nature of intracage jump, providing the first experimental confirmation of prior computational predictions. Importantly, our findings are distinct from the de Gennes narrowing scenario, often discussed in coherent QENS theory, where QENS widths narrow at wave vectors with strong $S(\mathbf{Q})$ intensity, reflecting long-lived metastable correlated configurations [68,72,73]. In superionic Cu_7PS_6, the coherent QENS spectra at diffuse lobes remains broad, reflecting very fast and continuous spatially correlated hopping dynamics. Such collective hopping is believed to underpin the facile ion transport in argyrodites, making them attractive SICs [10,30,32].

B. Spatial correlation of collective hopping

To gain real-space insight into Cu-Cu spatial correlations during the hopping process, we calculate the 3D Δ-PDF at 600 K, obtained from our diffuse scattering simulations over a large reciprocal space, up to 10 r.l.u. in each direction (Fig. S19 [52]). The 3D Δ-PDF encodes real-space ion-ion correlations, and its maxima reflect preferred bond vectors —it is the Fourier transform of the diffuse scattering observed in **Q** space with the correlations of the average crystal lattice subtracted [74–76]. We note that our measurements clearly capture the diffuse scattering features, providing experimental evidence for the underlying spatial correlations. However, limited **Q** coverage and background artifacts in neutron scattering measurements prevent a robust reconstruction of the 3D Δ-PDF, and we therefore resort to simulations. The resulting 3D Δ-PDF exhibits strong positive correlations along bond vectors forming a triangular patch, with local maxima at around $[0.15\,0.15\,0.25]$ in lattice unit (l.u.), and permutated coordinates [red patches in Fig. 2(i)]. Eight such patches, following the local symmetry of the cages, are located approximately 3 Å from the origin. These indicate the preferred Cu-Cu distance and bond directions maintained during hopping process. Consistently, the diffuse lobe at (2.5 2.5 0.5) has a wave-vector magnitude $|\mathbf{Q}| = 2.32$ Å^{-1}, corresponding to $d \approx 2.7$ Å in real space, matching the strong positive correlations revealed in the 3D Δ-PDF. From MLMD trajectories, we further identify collective intracage events for pairs of Cu ions moving along adjacent edges of a cage, while maintaining bond vectors consistent with the spatial correlations predicted by the 3D Δ-PDF [Fig. 2(j)]. Together, these findings reveal the dominant spatial correlations underlying collective hopping in Cu_7PS_6, which give rise to the observed diffuse scattering and coherent QENS. We also computed the correlation factor related to the Haven ratio from MLMD trajectories, yielding a value of 2.8 for Cu ions at 600 K, indicating that, on average, about three Cu ions hop collectively (Supplemental Material [52] Sec. VIII). Additional collective hopping events identified in our MLMD trajectories, including multi-ion hops, are shown in Fig. S20 [52].

IV. CONNECTION TO ANHARMONIC PHONONS

Next, we show how specific phonons activate fast collective hopping. Figures 3(a) and 3(b) compare the slices of $S(\mathbf{Q}, E)$ from LET along the $[2.5\,2.5\,L]$ direction,

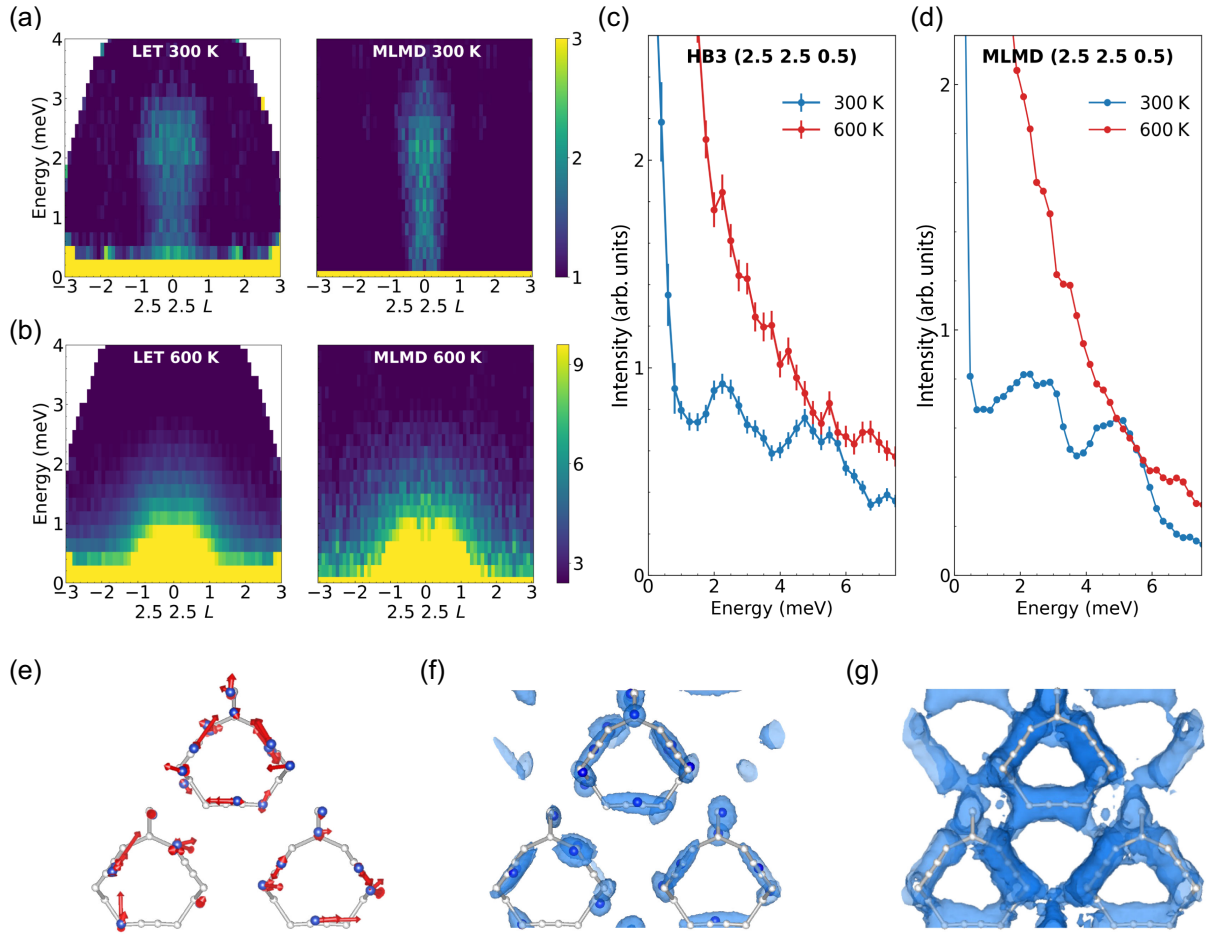

FIG. 3. Evolution from phonon vibrations to collective hopping across the superionic transition in Cu_7PS_6. (a)–(d) INS measurements and MLMD simulations reveal that the coherent QENS originates from the breakdown of low-energy optical phonons. $S(\mathbf{Q}, E)$ slices along the $[2.5\,2.5\,L]$ direction, measured by LET and simulated by MLMD at (a) 300 and (b) 600 K, together with energy spectra at $\mathbf{Q} = (2.5\,2.5\,0.5)$ from (c) HB3 measurements and (d) MLMD simulations. (e) Eigenvectors of the soft optical mode at $\mathbf{q} = (0.5\,0.5\,0.5)$ with 3.36 meV in the $P2_13$ phase. The phonon eigenvectors (red arrows) strongly overlap with the intracage pathway. (f) Probability density of Cu ions from configurations generated by the low-energy phonon modes. (g) Cu probability map from 600 K MLMD for comparison.

across the diffuse lobes, at 300 and 600 K. A broad maximum of intensity centered at about 2.5 meV at around (2.5 2.5 0) is observed at 300 K, reflecting that this phonon mode is already very soft and damped even at room temperature. This broad phonon evolves into the coherent QENS response in the superionic phase at 600 K, becoming overdamped as the vibrational dynamics become relaxational from stochastic jumps in time. Again, our MLMD simulations successfully capture this behavior. A clear evolution from low-energy phonons to coherent QENS is also observed in the energy spectra measured at (2.5 2.5 0.5) using HB3 at HFIR. As shown in Figs. 3(c) and 3(d), the low-energy phonon peak around 2.5 meV seen at 300 K evolves into a quasielastic response at 600 K. Figure S22 [52] compares the data from LET and HB3, cross-validating our observations.

We further trace these phonon modes to lower temperatures with HB3 and characterize their temperature evolution. Figure S23(a) [52] shows $S(E)$ spectra at $\mathbf{Q} = (2.5\,2.5\,0.5)$ from 50 to 600 K. At 50 K, well-defined low-energy optical phonon peaks are observed at approximately 3.5 and 6 meV, consistent with estimates from a heat capacity analysis [50]. As T increases, these phonon modes soften and broaden, eventually breaking down in the superionic phase. Notably, spectra of the 3.5 meV modes change dramatically even in the low-temperature range, reflecting the extremely soft bonding of the Cu ions with very shallow and anharmonic potentials. These lower-energy modes therefore correspond to large-amplitude vibrations of the Cu ions that approach the migration saddle points, evolving into the c-QENS response upon warming. The spectral weight transfer from low-energy phonons to diffusive dynamics across the superionic transition is reminiscent of prior investigations on other SICs based on powder-averaged $S(E)$ [26–29] and is also observed in our powder measurements [Fig. S23(b) [52]].

Beyond previous findings, here we identify the key phonon modes coupling to the superionic transition based on single-crystal INS and observe the breakdown of these modes as they evolve into coherent QENS and diffuse intensity in the superionic regime. These results highlight the intrinsic connection between phonon vibrations and collective hopping, with low-energy optical phonons of the parent normal phase representing precursor collective hopping modes. These soft phonons correspond to correlated Cu motions that align with the softest directions of the potential energy surface, enabling superionic diffusion via correlated hopping. The evolution from low-energy phonons to coherent QENS is further demonstrated in the computed $S(\mathbf{Q}, E)$ slices based on quasiharmonic approximation (QHA) and MLMD simulations at multiple T (Fig. S24 [52]). Importantly, MLMD allows us to separate the contributions from different ion pairs and establish that these dynamics are predominantly driven by cooperative motions of Cu cations.

Moreover, we can see that the phonon-activated collective hopping process is strongly modulated by the host lattice dynamics and contributes to long-range diffusion (see Supplemental Material [52] Sec. IX). This highlights the key role of lattice flexibility in ionic diffusion processes, supporting materials-design strategies based on tuning host-lattice dynamics [8,77]. In parallel, we also observe the emergence of a linear phonon DOS, $g(\omega) \sim \omega$, in the superionic phase, indicative of liquidlike dynamics (Fig. S26 [52]) [43,44]. This behavior echoes our recent observation in the Li argyrodite Li_6PS_5Cl (in powder samples) that revealed liquidlike dynamics via an excess low-energy spectral weight, although the specific overdamped phonons could not be identified [27]. The coherent QENS observed in Cu_7PS_6 underlies this spectral weight enhancement and pinpoints the origin of the liquidlike DOS.

Lastly, we establish the specific phonon modes that act as precursors to intracage jump in Cu_7PS_6 using on phonon eigenvector analysis. Figure 3(e) visualizes the eigenvectors of the lowest-energy phonon modes with 3.36 meV at the reduced $\mathbf{q}$ point (0.5 0.5 0.5) calculated by QHA. These modes correspond to the low-energy phonons observed at (2.5 2.5 0.5) in the LET and HB3 measurements. We find that the atomic displacements from these modes strongly overlap with the intracage pathways of Cu ions. By projecting the MLMD trajectories onto these modes and computing the mode-projected power spectrum, we clearly observe a well-defined phonon peak at low temperatures, which gradually broadens and eventually breakdowns upon warming across the superionic transition (Fig. S27 [52]). To further validate that these phonon modes act as a precursor to intracage jump, we generate Cu configurations compatible with these eigenvectors and compute the resulting Cu probability density. The resulting distribution closely resembles the intracage Cu density calculated from the 600 K MLMD simulations [Figs. 3(f) and 3(g)], further supporting our identification of the precursor phonons that facilitate intracage concerted jump.

V. CONCLUSION

Our study firmly establishes the prevalence of collective hopping in superionic argyrodites and traces its origin to specific low-frequency phonons, by combining comprehensive neutron scattering experiments with large-scale MLMD simulations resolving 4D spatiotemporal correlations of ionic motions. We decisively reveal the emergence of $\mathbf{Q}$-dependent diffuse scattering and coherent QENS in superionic Cu_7PS_6, providing experimental evidence of spatially correlated cation hops. Our results clearly reveal collective Cu ion hops along the edges of clusters, preserving a preferred bond distance and a set of bond vectors. Furthermore, we demonstrate that these collective intracage hops originate from the breakdown of specific phonon modes in the parent phase, establishing a microscopic connection between soft phonons along a shallow saddle point in the potential energy surface and concerted ionic migration. The cooperative hopping behavior identified herein goes beyond prior predictions and directly measures the key dynamic correlations enabling facile diffusion in argyrodites. Taken together, these results resolve prior controversies and reveal the dynamical origin of ionic diffusion, going beyond conventional considerations of static potential energy surfaces. The definite link established between precursor phonons and facile collective hops advances the fundamental understanding of ion transport and provides a physical basis for tuning relevant vibrational modes to shape transport properties in superionic materials.

ACKNOWLEDGMENTS

We thank Jingxuan Ding, Xing He, and Raymond Osborn for valuable discussions. Neutron scattering data collection, MD simulations, and analysis by H.-M. L. was supported by a U.S. National Science Foundation DMREF project under Award No. DMR-2119273. Neutron scattering experiments (T. W.) and first-principles modeling (N. O.) were supported by the U.S. Department of Energy (DOE), Office of Science, Basic Energy Sciences, Materials Sciences and Engineering Division, under Award No. DE-SC0023286. O. D. acknowledges Duke startup funds for the support of M. K. G. and Duke Pratt School of Engineering Beyond the Horizon partial support for N. O. Sample synthesis (powders) by M. T. R. and A. Z. was supported by the U.S. National Science Foundation DMREF project under Award No. DMR-2118463. Experiments at the ISIS Neutron and Muon Source were supported by a beam time allocation RB2320140 from the Science and Technology Facilities Council. The use of Oak Ridge National Laboratory's High

Flux Isotope Reactor and Spallation Neutron Source was sponsored by the Scientific User Facilities Division, Office of Basic Energy Sciences, U.S. DOE. The beam time was allocated to CTAX on Proposal No. IPTS-32982, WAND^2 on No. IPTS-32315, HB3 on No. IPTS-32303, and ARCS on No. IPTS-32965. Theoretical calculations were performed using the National Energy Research Scientific Computing Center, a U.S. DOE Office of Science User Facility supported by the Office of Science of the U.S. DOE under Contract No. DE-AC02-05CH11231.

O. D. and H.-M. L. designed the research. A. P. grew and characterized the single crystal. M. T. R. and A. Z. synthesized and characterized the powder sample. H.-M. L., T. W., J. R. S., F. J., T. H., Y. W., S. C., and D. L. A. performed neutron scattering measurements. H.-M. L., M. K. G., and N. O. performed simulations. H.-M. L. analyzed data. H.-M. L. and O. D. wrote the paper.

The authors declare that they have no competing interests.

DATA AVAILABILITY

All data needed to evaluate the conclusions in the paper are present in the paper and/or Supplemental Material [52]. Additional data related to this paper may be requested from the authors. The numerical data for the figures are available from the Duke open research repository [81]. The data from the LET experiments are available [82].

APPENDIX A: RESOLVING THE ATOMIC DYNAMICS THROUGH NEUTRON SCATTERING AND MOLECULAR DYNAMICS

The fundamental quantity describing atomic dynamics and correlations is the Van Hove correlation function $G(\mathbf{r},t)$, defined in Eqs. (1) and (2) in the main text. The Van Hove correlation function can be decomposed into a self part $G_s(\mathbf{r},t)$ and a distinct part $G_d(\mathbf{r},t)$, describing single-particle motion and spatial correlations between different atoms, respectively.

In neutron scattering experiments, the measured quantity is the dynamical structure factor $S(\mathbf{Q},E)$, which is the double Fourier transform of the Van Hove function in both time and space:

$$S(\mathbf{Q},E)=\frac{1}{2\pi\hbar}\int_{-\infty}^{\infty}e^{iEt/\hbar}dt\int e^{-i\mathbf{Q}\cdot\mathbf{r}}G(\mathbf{r},t)d\mathbf{r}. \quad \text{(A1)}$$

The measured $S(\mathbf{Q},E)$ has contributions from both the coherent dynamical structure factor $S^{IJ}_{\mathrm{coh}}(\mathbf{Q},E)$, which probes the correlated dynamics between the Ith and Jth elements, and the incoherent dynamical structure factor $S^{I}_{\mathrm{inc}}(\mathbf{Q},E)$, which probes the self-dynamics of the Ith element. They are defined as

$$S^{IJ}_{\mathrm{coh}}(\mathbf{Q},E)=\frac{1}{2\pi}\int_0^{\infty}\sum_{i,j}e^{-i\mathbf{Q}\cdot[\mathbf{R}_{I,i}(0)-\mathbf{R}_{J,j}(t)]}e^{iEt/\hbar}dt, \quad \text{(A2)}$$

$$S^{I}_{\mathrm{inc}}(\mathbf{Q},E)=\frac{1}{2\pi}\int_0^{\infty}\sum_{i}e^{-i\mathbf{Q}\cdot[\mathbf{R}_{I,i}(0)-\mathbf{R}_{I,i}(t)]}e^{iEt/\hbar}dt, \quad \text{(A3)}$$

where $\mathbf{R}_{I,i}(t)$ is the ith atom position of element type I at time t and the summation indices i and j represent the sum over the Ith and Jth types of elements, respectively. The indices I and J may be equal, in which case $S^{IJ}_{\mathrm{coh}}(\mathbf{Q},E)$ describes correlations between different atoms of the same element. The total measured neutron scattering intensity is thus proportional to

$$S_{\mathrm{tot}}(\mathbf{Q},E)\propto\sum_{I,J}b^{I}_{\mathrm{coh}}b^{J}_{\mathrm{coh}}S^{IJ}_{\mathrm{coh}}(\mathbf{Q},E)+\sum_{J}(b^{J}_{\mathrm{inc}})^2S^{J}_{\mathrm{inc}}(\mathbf{Q},E), \quad \text{(A4)}$$

where b^{I}_{coh} and b^{I}_{inc} are the coherent and incoherent scattering lengths of the Ith element, respectively, and the summation indices I and J run over different elements in the unit cell.

In addition to neutron scattering experiments, we performed large-scale molecular dynamics simulations, from which $S(\mathbf{Q},E)$ [or $G(\mathbf{r},t)$] can be directly computed from atomic trajectories, enabling direct comparison with neutron scattering measurements. For a detailed description of the methodology, see Supplemental Material [52].

APPENDIX B: COHERENT QENS AS A SIGNATURE OF COLLECTIVE HOPPING

Generally, coherent QENS reflects overdamped dynamics arising from spatially correlated displacements. It is not uniquely associated with collective hopping. It may also originate from damped structural fluctuations, as reported for metal halide perovskites even in the absence of ionic hopping [78,79]. In the present case of Cu_7PS_6, however, the coherent QENS signal emerges only in the superionic phase, when Cu ions begin to hop rapidly. This indicates that the observed signal originates from spatial correlations associated with the hopping process, namely, cooperative hopping of mobile ion pairs between different sites while maintaining short-range dynamical correlations. Similar coherent QENS signatures have previously been used to investigate collective hopping behavior in bulk water, ionic liquid systems, quasicrystals, and fluoride conductors [64–68]. In the case of purely uncorrelated self-diffusion, the relative phases of the scattered neutron wavelets would become randomized and therefore would not produce the constructive interference responsible for the observed $\mathbf{Q}$ modulation of diffuse intensity maxima and coherent QENS.

Furthermore, the simultaneous observation of diffuse scattering and a QENS response in a superionic system does not by itself imply collective diffusion, since diffuse scattering may arise from static disorder of the host lattice [80], while incoherent QENS may originate from self-diffusion in a disordered system [22]. Here, the $\mathbf{Q}$-dependent diffuse intensity arises from a coherent QENS response associated specifically with the mobile ions, reflecting short-range dynamic Cu-Cu correlations. We stress that the diffuse pattern observed in $S(\mathbf{Q})$ in Fig. 1(e) originates from the coherent QENS response, since the signal is integrated over the energy window $|E| \leq 1$ meV, which includes the quasielastic contribution and therefore reflects the underlying dynamic correlations.

Taken together, our single-crystal neutron scattering measurements directly resolve both the spatial and temporal aspects of the correlated Cu-ion dynamics in superionic Cu_7PS_6. The observed coherent QENS response provides access to both the hopping characteristics and the underlying correlation vectors. As discussed in Sec. III, we match the observed coherent QENS signal to the intracage hopping process, evidencing cooperative hopping of Cu ions within the cage.

[1] James B. Boyce and Bernardo A. Huberman, *Superionic conductors: Transitions, structures, dynamics*, Phys. Rep. **51**, 189 (1979).

[2] Stephen Hull, *Superionics: Crystal structures and conduction processes*, Rep. Prog. Phys. **67**, 1233 (2004).

[3] Noriaki Kamaya, Kenji Homma, Yuichiro Yamakawa, Masaaki Hirayama, Ryoji Kanno, Masao Yonemura, Takashi Kamiyama, Yuki Kato, Shigenori Hama, Koji Kawamoto *et al.*, *A lithium superionic conductor*, Nat. Mater. **10**, 682 (2011).

[4] Sossina M. Haile, Dane A. Boysen, Calum R. I. Chisholm, and Ryan B. Merle, *Solid acids as fuel cell electrolytes*, Nature (London) **410**, 910 (2001).

[5] Yuntong Zhu, Juan Carlos Gonzalez-Rosillo, Moran Balaish, Zachary D. Hood, Kun Joong Kim, and Jennifer L. M. Rupp, *Lithium-film ceramics for solid-state lithionic devices*, Nat. Rev. Mater. **6**, 313 (2021).

[6] KyuJung Jun, Yu Chen, Grace Wei, Xiaochen Yang, and Gerbrand Ceder, *Diffusion mechanisms of fast lithium-ion conductors*, Nat. Rev. Mater. **9**, 887 (2024).

[7] Guopeng Han, Andrij Vasylenko, Luke M. Daniels, Chris M. Collins, Lucia Corti, Ruiyong Chen, Hongjun Niu, Troy D. Manning, Dmytro Antypov, Matthew S. Dyer *et al.*, *Superionic lithium transport via multiple coordination environments defined by two-anion packing*, Science **383**, 739 (2024).

[8] Zhantao Liu, Po-Hsiu Chien, Shuo Wang, Shaowei Song, Mu Lu, Shuo Chen, Shuman Xia, Jue Liu, Yifei Mo, and Hailong Chen, *Tuning collective anion motion enables superionic conductivity in solid-state halide electrolytes*, Nat. Chem. **16**, 1584 (2024).

[9] M Xu, J. Ding, and E. Ma, *One-dimensional stringlike cooperative migration of lithium ions in an ultrafast ionic conductor*, Appl. Phys. Lett. **101**, 031901 (2012).

[10] Xingfeng He, Yizhou Zhu, and Yifei Mo, *Origin of fast ion diffusion in super-ionic conductors*, Nat. Commun. **8**, 15893 (2017).

[11] Bingkai Zhang, Luyi Yang, Lin-Wang Wang, and Feng Pan, *Cooperative transport enabling fast Li-ion diffusion in Thio-LISICON* $Li_{10}SiP_2S_{12}$ *solid electrolyte*, Nano Energy **62**, 844 (2019).

[12] Zheyi Zou, Nan Ma, Aiping Wang, Yunbing Ran, Tao Song, Yao Jiao, Jinping Liu, Hang Zhou, Wei Shi, Bing He *et al.*, *Relationships between* Na+ *distribution, concerted migration, and diffusion properties in rhombohedral NASICON*, Adv. Energy Mater. **10**, 2001486 (2020).

[13] Aris Marcolongo and Nicola Marzari, *Ionic correlations and failure of Nernst-Einstein relation in solid-state electrolytes*, Phys. Rev. Mater. **1**, 025402 (2017).

[14] Cibrán López, Riccardo Rurali, and Claudio Cazorla, *How concerted are ionic hops in inorganic solid-state electrolytes?*, J. Am. Chem. Soc. **146**, 8269 (2024).

[15] Yirong Gao, Adelaide M. Nolan, Peng Du, Yifan Wu, Chao Yang, Qianli Chen, Yifei Mo, and Shou-Hang Bo, *Classical and emerging characterization techniques for investigation of ion transport mechanisms in crystalline fast ionic conductors*, Chem. Rev. **120**, 5954 (2020).

[16] K Funke, *Ion dynamics and correlations: Translational and localized ionic hopping motion in solid electrolytes*, Philos. Mag. A **68**, 711 (1993).

[17] Andrey D. Poletayev, Matthias C. Hoffmann, James A. Dawson, Samuel W. Teitelbaum, Mariano Trigo, M. Saiful Islam, and Aaron M. Lindenberg, *The persistence of memory in ionic conduction probed by nonlinear optics*, Nature (London) **625**, 691 (2024).

[18] Léon Van Hove, *Correlations in space and time and born approximation scattering in systems of interacting particles*, Phys. Rev. **95**, 249 (1954).

[19] Rolf Hempelmann, *Quasielastic Neutron Scattering and Solid State Diffusion* (Oxford University Press, New York, 2000).

[20] Tasso Springer, *Quasielastic Neutron Scattering for the Investigation of Diffusive Motions in Solids and Liquids*, Springer Tracts in Modern Physics Volume 64 (Springer, Berlin, Heidelberg, 2006), pp. 1–100.

[21] Naresh C. Osti, Niina Jalarvo, and Eugene Mamontov, *Backscattering silicon spectrometer (BASIS): Sixteen years in advanced materials characterization*, Mater. Horiz. **11**, 4535 (2024).

[22] Bettina Schwaighofer, Miguel A. Gonzalez, Mark R. Johnson, John S. O. Evans, and Ivana Radosavljević Evans, *Ionic mobility in energy materials: Through the lens of quasielastic neutron scattering*, Chem. Mater. **37**, 3575 (2025).

[23] J. M. Rowe, J. J. Rush, L. A. De Graaf, and G. A. Ferguson, *Neutron quasielastic scattering study of hydrogen diffusion in a single crystal of palladium*, Phys. Rev. Lett. **29**, 1250 (1972).

[24] Masato Matsuura, Yasuyuki Fujiwara, Hiroki Moriwake, Koji Ohara, and Yukinobu Kawakita, *Microscopic dynamics of lithium diffusion in single crystal of the solid-state*

electrolyte $La_{2/3-x}Li_3 \times TiO_3$ *(*$x = 0.13$*) studied by quasielastic neutron scattering*, Phys. Rev. B **104**, 094305 (2021).

[25] Sawankumar V. Patel, Swastika Banerjee, Haoyu Liu, Pengbo Wang, Po-Hsiu Chien, Xuyong Feng, Jue Liu, Shyue Ping Ong, and Yan-Yan Hu, *Tunable lithium-ion transport in mixed-halide argyrodites* $Li_{6-x}Ps_{5-x}ClBr_x$*: An unusual compositional space*, Chem. Mater. **33**, 1435 (2021).

[26] Qingyong Ren, Mayanak K. Gupta, Min Jin, Jingxuan Ding, Jiangtao Wu, Zhiwei Chen, Siqi Lin, Oscar Fabelo, Jose Alberto Rodríguez-Velamazán, Maiko Kofu *et al.*, *Extreme phonon anharmonicity underpins superionic diffusion and ultralow thermal conductivity in argyrodite* Ag_8SnSe_6, Nat. Mater. **22**, 999 (2023).

[27] Jingxuan Ding, Mayanak K. Gupta, Carolin Rosenbach, Hung-Min Lin, Naresh C. Osti, Douglas L. Abernathy, Wolfgang G. Zeier, and Olivier Delaire, *Liquid-like dynamics in a solid-state lithium electrolyte*, Nat. Phys. **21**, 118 (2025).

[28] Mayanak K. Gupta, Jingxuan Ding, Dipanshu Bansal, Douglas L. Abernathy, Georg Ehlers, Naresh C. Osti, Wolfgang G. Zeier, and Olivier Delaire, *Strongly anharmonic phonons and their role in superionic diffusion and ultralow thermal conductivity of* Cu_7PSe_6, Adv. Energy Mater. **12**, 2200596 (2022).

[29] Xingchen Shen, Michael Marek Koza, Yung-Hsiang Tung, Niuchang Ouyang, Chun-Chuen Yang, Chen Wang, Yue Chen, Kristin Willa, Rolf Heid, Xiaoyuan Zhou *et al.*, *Soft phonon mode triggering fast Ag diffusion in superionic argyrodite* Ag_8GeSe_6, Small **19**, 2305048 (2023).

[30] Benjamin J. Morgan, *Mechanistic origin of superionic lithium diffusion in anion-disordered* Li_6PS_{5x} *argyrodites*, Chem. Mater. **33**, 2004 (2021).

[31] Marcel Sadowski and Karsten Albe, *Influence of Br-/*S^{2-}*-site-exchange on li diffusion mechanism in* Li_6PS_5Br*: A computational study*, Phil. Trans. R. Soc. A **379**, 20190458 (2021).

[32] Byeongsun Jun and Sang Uck Lee, *Designing a descriptor for the computational screening of argyrodite-based solid-state superionic conductors: Uniformity of ion-cage size*, J. Mater. Chem. A **10**, 7888 (2022).

[33] Sokseiha Muy, Roman Schlem, Yang Shao-Horn, and Wolfgang G. Zeier, *Phonon–ion interactions: Designing ion mobility based on lattice dynamics*, Adv. Energy Mater. **11**, 2002787 (2021).

[34] Tao Song, Yuxiao Lin, Da Wang, Qianli Chen, Chen Ling, and Siqi Shi, *Renewing fundamental understanding of ionic transport in inorganic crystalline solid-state electrolytes from the perspective of lattice dynamics*, Adv. Energy Mater. 2302440 (2024).

[35] Marvin A. Kraft, Sean P. Culver, Mario Calderon, Felix Bocher, Thorben Krauskopf, Anatoliy Senyshyn, Christian Dietrich, Alexandra Zevalkink, Jurgen Janek, and Wolfgang G. Zeier, *Influence of lattice polarizability on the ionic conductivity in the lithium superionic argyrodites* Li_6PS_{5x} *(*$x =$ Cl*, Br, i)*, J. Am. Chem. Soc. **139**, 10909 (2017).

[36] Sokseiha Muy, John C. Bachman, Livia Giordano, Hao-Hsun Chang, Douglas L. Abernathy, Dipanshu Bansal, Olivier Delaire, Satoshi Hori, Ryoji Kanno, Filippo Maglia *et al.*, *Tuning mobility and stability of lithium ion conductors based on lattice dynamics*, Energy Environ. Sci. **11**, 850 (2018).

[37] Jennifer L. Niedziela, Dipanshu Bansal, Andrew F. May, Jingxuan Ding, Tyson Lanigan-Atkins, Georg Ehlers, Douglas L. Abernathy, Ayman Said, and Olivier Delaire, *Selective breakdown of phonon quasiparticles across superionic transition in* $CuCrSe_2$, Nat. Phys. **15**, 73 (2019).

[38] Mayanak Kumar Gupta, Sajan Kumar, Ranjan Mittal, and Samrath L. Chaplot, *Soft-phonon anharmonicity, Floppy modes, and Na diffusion in* Na_3PY *(*$Y =$ S*, Se, Te): Ab initio and machine-learned molecular dynamics simulations*, Phys. Rev. B **106**, 014311 (2022).

[39] Cibrán López, Agustí Emperador, Edgardo Saucedo, Riccardo Rurali, and Claudio Cazorla, *Universal ion-transport descriptors and classes of inorganic solid-state electrolytes*, Mater. Horiz. **10**, 1757 (2023).

[40] Zhizhen Zhang and Linda F. Nazar, *Exploiting the paddle-wheel mechanism for the design of fast ion conductors*, Nat. Rev. Mater. **7**, 389 (2022).

[41] KyuJung Jun, Byungju Lee, Ronald L. Kam, and Gerbrand Ceder, *The nonexistence of a paddlewheel effect in superionic conductors*, Proc. Natl. Acad. Sci. U.S.A. **121**, e2316493121 (2024).

[42] Jeffrey G. Smith and Donald J. Siegel, *A proper definition of the paddlewheel effect affirms its existence*, Proc. Natl. Acad. Sci. U.S.A. **122**, e2419892122 (2025).

[43] Alessio Zaccone and Matteo Baggioli, *Universal law for the vibrational density of states of liquids*, Proc. Natl. Acad. Sci. U.S.A. **118**, e2022303118 (2021).

[44] Caleb Stamper, David Cortie, Zengji Yue, Xiaolin Wang, and Dehong Yu, *Experimental confirmation of the universal law for the vibrational density of states of liquids*, J. Phys. Chem. Lett. **13**, 3105 (2022).

[45] T. Keyes, *Unstable instantaneous normal modes and diffusion in supercooled liquids*, J. Appl. Phys. **137**, 074702 (2025).

[46] Kunio Wakamura, *Roles of phonon amplitude and low-energy optical phonons on superionic conduction*, Phys. Rev. B **56**, 11593 (1997).

[47] Samuel M. Greene and Donald J. Siegel, *Assessing correlations between phonon features and cation migration barriers in multivalent solid electrolytes*, Chem. Mater. **36**, 7476 (2024).

[48] D. G. Sangiovanni, J. Klarbring, D. Smirnova, N. V. Skripnyak, D. Gambino, M. Mrovec, S. I. Simak, and I. A. Abrikosov, *Superioniclike diffusion in an elemental crystal: BCC titanium*, Phys. Rev. Lett. **123**, 105501 (2019).

[49] Ihor P. Studenyak, V. Yu Izai, Artem I. Pogodin, Oleksandr P. Kokhan, Vasil I. Sidey, M. Yu Sabov, Algimantas Kežionis, Tomas Šalkus, and Jūras Banys, *Structural and electrical properties of argyrodite-type* Cu_7PS_6 *crystals*, Lith. J. Phys. **57**, 243 (2017).

[50] Xingchen Shen, Niuchang Ouyang, Yuling Huang, Yung-Hsiang Tung, Chun-Chuen Yang, Muhammad Faizan, Nicolas Perez, Ran He, Andrei Sotnikov, Kristin Willa *et al.*, *Amorphous-like ultralow thermal transport in crystalline argyrodite* Cu_7PS_6, Adv. Sci. **11**, 2400258 (2024).

[51] Varley F. Sears, *Neutron scattering lengths and cross sections*, Neutron News **3**, 26 (1992).

[52] See Supplemental Material at http://link.aps.org/supplemental/10.1103/lx5w-x6wl for experimental and computational details, additional discussion, and supporting figures, which includes Refs. [10,13,16,26–28,49–50,53–62].

[53] Owen Arnold, Jean-Christophe Bilheux, J. M. Borreguero, Alex Buts, Stuart I. Campbell, L. Chapon, Mathieu Doucet, N. Draper, R. Ferraz Leal, M. A. Gigg *et al.*, *Mantid—Data analysis and visualization package for neutron scattering and μ sr experiments*, Nucl. Instrum. Methods Phys. Res., Sect. A **764**, 156 (2014).

[54] R. A. Ewings, A. Buts, M. D. Le, J. Van Duijn, I. Bustinduy, and T. G. Perring, *Horace: Software for the analysis of data from single crystal spectroscopy experiments at time-of-flight neutron instruments*, Nucl. Instrum. Methods Phys. Res., Sect. A **834**, 132 (2016).

[55] Georg Kresse and Jürgen Furthmüller, *Efficiency of ab-initio total energy calculations for metals and semiconductors using a plane-wave basis set*, Comput. Mater. Sci. **6**, 15 (1996).

[56] Georg Kresse and Daniel Joubert, *From ultrasoft pseudopotentials to the projector augmented-wave method*, Phys. Rev. B **59**, 1758 (1999).

[57] John P. Perdew, Kieron Burke, and Matthias Ernzerhof, *Generalized gradient approximation made simple*, Phys. Rev. Lett. **77**, 3865 (1996).

[58] Han Wang, Linfeng Zhang, Jiequn Han, and E. Weinan, *DeePMD-kit: A deep learning package for many-body potential energy representation and molecular dynamics*, Comput. Phys. Commun. **228**, 178 (2018).

[59] James Weng, Eric D. Dill, James D. Martin, Ross Whitfield, Christina Hoffmann, and Feng Ye, *K-space algorithmic reconstruction (KAREN): A robust statistical methodology to separate Bragg and diffuse scattering*, Appl. Crystallogr. **53**, 159 (2020).

[60] Niek J. J. De Klerk, Irek Roslon, and Marnix Wagemaker, *Diffusion mechanism of Li argyrodite solid electrolytes for Li-ion batteries and prediction of optimized halogen doping: The effect of Li vacancies, halogens, and halogen disorder*, Chem. Mater. **28**, 7955 (2016).

[61] I Hanghofer, M. Brinek, S. L. Eisbacher, B. Bitschnau, M. Volck, V. Hennige, I. Hanzu, D. Rettenwander, and H. M. R. Wilkening, *Substitutional disorder: Structure and ion dynamics of the argyrodites* Li_6Ps_5Cl, Li_6Ps_5Br *and* Li_6Ps_5I, Phys. Chem. Chem. Phys. **21**, 8489 (2019).

[62] Jiho Lee, Suyeon Ju, Seungwoo Hwang, Jinmu You, Jisu Jung, Youngho Kang, and Seungwu Han, *Disorder-dependent Li diffusion in* Li_6Ps_5Cl *investigated by machine-learning potential*, ACS Appl. Mater. Interfaces **16**, 46442 (2024).

[63] Gordon Leslie Squires, *Introduction to the Theory of Thermal Neutron Scattering* (Courier Corporation, North Chelmsford, MA, 1996).

[64] Margarita Russina, Gerrit Gunther, Bela Farago, Earl Babcock, Zahir Salhi, Alexander Ioffe, and Ferenc Mezei, *Structural fluctuations at nanoscale and cooperative molecular dynamics in bulk water*, J. Phys. Chem. Lett. **16**, 5835 (2025).

[65] Holger Euchner, Tsunetomo Yamada, Helmut Schober, Stephane Rols, Marek Mihalkovič, Ryuji Tamura, Tsutomu Ishimasa, and Marc de Boissieu, *Ordering and dynamics of the central tetrahedron in the* 1/1 Zn_6Sc *periodic approximant to quasicrystal*, J. Phys. Condens. Matter **24**, 415403 (2012).

[66] Holger Euchner, Tsunetomo Yamada, S. Rols, Tsutomu Ishimasa, Y. Kaneko, Jacques Ollivier, H. Schober, M. Mihalkovic, and M. De Boissieu, *Tetrahedron dynamics in the icosahedral quasicrystals i-ZnMgSc and i-ZnAgSc and the cubic* 1/1*-approximant* Zn_6Sc, J. Phys. Condens. Matter **25**, 115405 (2013).

[67] Tatsiana Burankova, Rolf Hempelmann, Andrew Wildes, and Jan P. Embs, *Collective ion diffusion and localized single particle dynamics in pyridinium-based ionic liquids*, J. Phys. Chem. B **118**, 14452 (2014).

[68] Jared Coles, Omar Chmaissem, Matthew Krogstad, Daniel M. Pajerowski, Feng Ye, Duck Young Chung, Mercouri G. Kanatzidis, Stephan Rosenkranz, and Raymond Osborn, *Four-dimensional quasielastic neutron scattering (4D-QENS) analysis of correlated ionic conduction in* $SrCl_2$, PRX Energy **5**, 023002 (2026).

[69] R. M. Moon, T. Riste, and W. C. Koehler, *Polarization analysis of thermal-neutron scattering*, Phys. Rev. **181**, 920 (1969).

[70] C. T. Chudley and R. J. Elliott, *Neutron scattering from a liquid on a jump diffusion model*, Proc. Phys. Soc. London **77**, 353 (1961).

[71] Shriparna Mukherjee, David J. Voneshen, Andrew Duff, Pooja Goddard, Anthony V. Powell, and Paz Vaqueiro, *Beyond rattling: Tetrahedrites as incipient ionic conductors*, Adv. Mater. **35**, 2306088 (2023).

[72] P. G. De Gennes, *Liquid dynamics and inelastic scattering of neutrons*, Physica (Amsterdam) **25**, 825 (1959).

[73] S. K. Sinha and D. K. Ross, *Self-consistent density response function method for dynamics of light interstitials in crystals*, Physica (Amsterdam) **149B+C**, 51 (1988).

[74] Thomas Weber and Arkadiy Simonov, *The three-dimensional pair distribution function analysis of disordered single crystals: Basic concepts*, Z. Kristallographie **227**, 238 (2012)..

[75] Matthew J. Krogstad, Stephan Rosenkranz, Justin M. Wozniak, Guy Jennings, Jacob P. C. Ruff, John T. Vaughey, and Raymond Osborn, *Reciprocal space imaging of ionic correlations in intercalation Compounds*, Nat. Mater. **19**, 63 (2020).

[76] Thomas Richard Welberry, *Diffuse X-Ray Scattering and Models of Disorder* (Oxford University Press, New York, 2022), Vol. 31.

[77] Kim H. Pham, Vijaya Begum-Hudde, Amy K. Lin, Natan A. Spear, Jackson McClellan, Michael W. Zuerch, Andre Schleife, Kimberly A. See, and Scott K. Cushing, *The dynamical role of optical phonons and sublattice screening in a solid-state ion conductor*, J. Am. Chem. Soc. **147**, 26456 (2025).

[78] Tyson Lanigan-Atkins, Xing He, M. J. Krogstad, D. M. Pajerowski, Douglas L. Abernathy, Guangyong N. M. N. Xu, Zhijun Xu, D.-Y. Chung, M. G. Kanatzidis, Stephan Rosenkranz *et al.*, *Two-dimensional overdamped fluctuations of the soft perovskite lattice in* $CsPbBr_3$, Nat. Mater. **20**, 977 (2021).

[79] Chengjie Mao, Xing He, Hung-Min Lin, Mayanak K. Gupta, Patrick Postec, Tyson Lanigan-Atkins, Matthew

Krogstad, Daniel M. Pajerowski, Tao Hong, Travis J. Williams *et al.*, *Correlated dynamic disorder, octahedral tilts, and acoustic phonon softening in* $CsSnBr_3$ *and* $CsPbBr_3$, Phys. Rev. Mater. **9**, 065401 (2025).

[80] Yu Chen, Caleb Ramette, Matthew Krogstad, Maxim Avdeev, Erick Lawrence, Satya Kushwaha, Chao-Chun Wei, Rajavallipuram Sankaran Subramanian, Birender Singh, Bin Liu *et al.*, *Framework short-range order observed in a spinel-type Li superionic conductor*, J. Am. Chem. Soc. **148**, 9244 (2026).

[81] 10.7924/r4r540.

[82] 10.5286/ISIS.E.RB2320140.